NASA Technical Memorandum 81541

INFLUENCE OF PRESSURE DRIVEN SECONDARY FLOWS ON THE BEHAVIOR OF TURBOFAN FORCED MIXERS

B. Anderson, L. Povinelli,
and W. Gerstenmaier
Lewis Research Center
Cleveland, Ohio

Prepared for the
Sixteen Joint Propulsion Conference
cosponsored by the AIAA, ASME, and SAE
Hartford, Connecticut, June 30-July 2, 1980

NASA

INFLUENCE OF PRESSURE DRIVEN SECONDARY FLOWS ON THE BEHAVIOR OF TURBOFAN FORCED MIXERS

by B. Anderson, L. Povinelli, and W. Gerstenmaier

National Aeronautics and Space Administration
Lewis Research Center
Cleveland, Ohio 44135

SUMMARY

An analytical and experimental study was performed to determine the influence of pressure driven secondary flows on the behavior of turbofan forced mixer nozzles. The basic secondary flow structure entering the nozzle was identified experimentally and was composed of a strong vortex system aligned with the radial interface between the fan and core streams. A generic secondary flow vortex structure was constructed for input to the analysis to represent the large scale structure of this inflow condition. Comparison between experiment and analysis at five axial stations showed very good agreement and indicated that this vortex system was convected downstream and dominated the mixing process.

NOMENCLATURE

E	energy
h	metric coefficient
i	unit vector
k	turbulent kinetic energy
Pr	Prandtl number
Q	magnitude of $\bar{U}$, equal to $(u^2 + v^2 + w^2)$
Re	Reynolds number
$\bar{U}$	velocity vector
u	primary velocity
v,w	secondary velocities
x,y,z	three component directions
γ	specific heat ratio
μ	viscosity
ε	turbulent dissipation

ξ vorticity

ρ density

ϕ velocity potential

ψ stream function

Subscripts:

I inviscid component

p primary component

s secondary component

T turbulent

v viscous component

ϕ irrotational component

ψ rotation

1,2,3 components in x,y,z direction

INTRODUCTION

It has long been known that mixing the hot core stream with the cooler fan stream of a turbofan engine prior to expansion through the exhaust nozzle can result in significant performance gains. The level of these gains depends on the trade-offs between the degree of mixing of the two streams and the viscous losses incurred in the mixing process. Of the many devices that have been used to promote mixing, the lobe mixer has clearly been most successful.

To date, the performance of lobe mixers has been determined almost entirely through experimentation.[1],[2],[3] These experiments were sufficient to determine the relative merits of one lobe configuration over another. However, in the absence of any clear understanding of the mixing process, conclusions reached with one series of tests could not be generalized to the next generation of mixer nozzles. Fluid flow analysis for the design of turbofan mixer nozzles was first published by Birch, Paynter, Spalding and Tatchell[4] and showed encouraging results. However, the role of various aerodynamic processes which take place within the mixer nozzles was clearly still not understood. It was first suggested in the Lewis Aeropropulsion 1979 Conference and later by Povinelli, Anderson and Gerstenmaier[6] that convective forces arising from pressure driven secondary flows play a far more important role in the mixing processes than first anticipated. These convective forces arise due to secondary flows at entry, which are sustained in the mixer passage by transverse pressure gradients that deflect the mean flow.

A major reason for the lack of detailed information about the character of the flows within the mixer nozzle passage stems from measurement difficulties

which have been partly removed by the development of the Laser-Doppler Velocimeter, which was used to take three component velocity measurements[7] in such configurations. These measurements strongly support the existance of large pressure driven secondary flows which can greatly influence the performance of turbofan mixer nozzles and help explain the often conflicting experimental results that have been reported.[6] In addition to the laser experiments, flow angularity measurements have been performed, and are described in a later section. This paper utilizes the new angularity data and delves further into the question of the influence of pressure driven secondary flows on the characteristics of turbofan mixer nozzles. The ramifications of such flows with regard to analytical modeling and their importance within the design process are investigated, along with the identification of the relevant parameters associated with the mixing process.

ANALYSIS

A. Governing Equations

The calculational procedure used in this study of forced mixer nozzle flow fields is an application of the approach developed by Briley, McDonald and Kreskovsky[8,9] and is designated PEPSIM. The procedure is based on the decomposition of the velocity field into primary and secondary flow velocities. Equations governing the streamwise development of the primary and secondary flow velocity fields are solved by an efficient algorithm using both block and scalar ADI methods. Although the governing equations are solved by a forward marching method, elliptic effects due to curvature and area change are accounted for a-priori through the imposed pressure gradients determined from a potential flow solution for the geometry in question. Since the primary concern in the lobe mixer problem is thermal mixing of the fan and core streams to achieve thrust augmentation, an energy equation is introduced.

B. The Turbulence Models

For turbulent flows, the turbulent viscosity which appears in the governing equations must be specified. Two types of turbulent models are used in PEPSIM to determine turbulent viscosity; a two equation k-ε turbulence model as presented by Launder and Spaulding[10] and a wake-turbulence model. In the orthogonal coordinate system and with the approximations required for a forward marching solution, the equations governing turbulent kinetic energy and dissipation for the k-ε model are given by

$$\rho u h_2 h_3 \frac{\partial k}{\partial x} + \rho v_s h_1 h_3 \frac{\partial k}{\partial y} + \rho w_s h_1 h_2 \frac{\partial k}{\partial z} = \frac{1}{Re}\left\{\frac{\partial}{\partial y}\left[\frac{h_1 h_3}{h_2}\left(\mu + \frac{\mu_T}{\sigma_k}\right)\frac{\partial k}{\partial y}\right]\right.$$

$$\left. + \frac{h_1 h_2}{h_3}\frac{\partial}{\partial z}\left[\left(\mu + \frac{\mu_T}{\sigma_k}\right)\frac{\partial k}{\partial z}\right]\right\} - h_1 h_2 h_3 \rho\varepsilon + p$$

$$\rho u h_2 h_3 \frac{\partial \varepsilon}{\partial x} + \rho v_s h_1 h_3 \frac{\partial \varepsilon}{\partial y} + \rho w_s h_1 h_2 \frac{\partial \varepsilon}{\partial z} = \frac{1}{Re} \left\{ \frac{\partial}{\partial y} \left[\frac{h_1 h_3}{h_2} \left(\mu + \frac{\mu_T}{\sigma_\varepsilon} \right) \frac{\partial \varepsilon}{\partial y} \right] \right.$$

$$\left. + \frac{h_1 h_2}{h_3} \frac{\partial}{\partial z} \left[\left(\mu + \frac{\mu_T}{\sigma_\varepsilon} \right) \frac{\partial \varepsilon}{\partial z} \right] \right\} - h_1 h_2 h_3 C_2 \rho \frac{\varepsilon^2}{k} + C_1 \frac{\varepsilon}{k} P$$

where k is the turbulent kinetic energy, ε is the turbulent dissipation and P represents the turbulent production given as:

$$P = \mu_T \left(\frac{1}{h_2} \frac{\partial u}{\partial y} \right)^2 + \left(\frac{1}{h_2} \frac{\partial w}{\partial y} \right)^2 + \left(\frac{1}{h_3} \frac{\partial u}{\partial z} \right)^2 + \left(\frac{1}{h_3} \frac{\partial v}{\partial z} \right)^2$$

The constants appearing in these equations are assigned their usual values of $C_1 = 1.44$, $C_2 = 1.92$, $C_\mu = 0.09$, $b_k = 1.0$ and $b_\varepsilon = 1.3$. These equations are solved independent of the fluid equations using a linear block implicit (LBI) scheme. The turbulent viscosity is then determined from k and ε by the relationship

$$\mu_T = \frac{C_\mu \rho k^2}{\varepsilon} Re$$

In the wake-turbulence model, the assumption is made that the turbulent velocity and length scales are frozen at their initial value. Thus, the turbulent viscosity is proportional to density.

C. Specification of Initial (Inflow) Conditions

Specification of the initial (inflow) conditions for a lobe mixer calculation in PEPSIM may be performed either by specifying the initial values of the velocity and temperature field or by using an automated procedure which constructs the initial velocity and temperature fields parametrically. In either case it is unlikely that the specified velocity field would be compatible with the continuity equations. Therefore, this velocity field is modified in a way that makes it compatible with the continuity equation while at the same time maintaining the initial secondary flow vorticity unaltered. The processing of the velocity field is performed in the following manner. The streamwise momentum equation is solved to obtain approximate values for the streamwise velocity gradients. The secondary flow vorticity is computed from the specified velocity field. A scalar potential is then constructed and solved yielding the irrotational components of the secondary flow which balance the streamwise velocity gradient in the continuity equation. Finally, a vector potential is constructed using the initial secondary flow vorticity and solved yielding the irrotational components of the secondary flow. Due to the nature of the vector potential these velocity components do not effect the continuity balance obtained from the scalar potential. The resulting velocity field is compatible with the continuity equation to first order in the marching direction.

EXPERIMENTAL APPARATUS

The test apparatus used has been described in a previous paper[6] and consisted of two basic parts: a fixed upstream model section and a rotating shroud, figure 1. The upstream section simulated the flow path through a typical high by-pass turbofan engine. A cross-section of the model is shown in figure 2. Heated air was supplied to the core passage and flowed through the lobe section. Unheated air was supplied to the fan passage and flowed around the lobe section which was interchangeable. In this paper, only the results obtained with one mixer section are presented and this configuration had a penetration (lobe tip radius/shroud radius) of 0.822 and the circumferential spacing ratio (core included angle/fan included angle) of 0.5. The ratio of the shroud length to the inside shroud diameter (at the lobe exit plane) was 0.71.

Total pressure and temperature measurements were made upstream in both the fan and core flows. Instrumentation rakes were also mounted in the rotating shroud for probing the mixer flow field (see fig. 2). Total temperature rakes were located at five axial stations in the mixing region. The first station was at the lobe exit plane, the second was halfway to the end of the plug, the third was at the end of the plug, the fourth was midway between the plug end and the nozzle exit, and the fifth station was at the nozzle exit plane. The rakes at the lobe and nozzle exit stations as well as the rotating mechanism are shown in figure 1. Total pressures were also measured at the lobe and nozzle exit stations. The temperature data were obtained over a 54 degree segment in 3 degree increments at 14 radial positions. Flow angularity measurements using the fixed probe technique[11] were made at the two locations shown in figure 2. The first measuring station was at the lobe exit plane; the second at the end of the centerbody. A photograph of the angularity rakes are shown in figure 3. Each rake has six probes and each probe has three tubes. The center tube is a chambered total pressure probe and the two side (upper and lower) tubes have a 45 degree sweepback. The pressure difference between the two side probes and the indicated total pressure were used along with a calibration curve in order to obtain flow directions (radial and azimuthal). Each probe was individually calibrated in an open jet at a Mach number of 0.45. The radial probe was set at various pitch angles to the flow and the azimuthal probe at various yaw angles. The indicated total pressure and the differences in side tube (upper-lower) pressures were used to establish a calibration curve.

Wall static pressure measurements completed the information needed to compute a resultant velocity. The resultant velocity was then used with the radial and azimuthal flow angles to compute the three velocity components.

The fan and core streams were operated with a total pressure ratio of one and a total temperature ratio of 0.74. The Mach number of the fan and core streams at the mixing plane (lobe exit) was approximately 0.45 and the by-pass ratio was 4.

COMPUTATIONAL PROCEDURE

A. Computational Mesh

In this section, specific details arising from the application of the foregoing analysis to the turbofan mixer configuration described earlier is given. The cross-section of this mixer geometry is presented in figure 4. The area immediately downstream of the nozzle plug tip is faired in with an assumed streamline to model the separated flow region expected in this mixer nozzle. Since the flow area excluded from consideration is small, this treatment is not believed to introduce significant error. The curvilinear coordinate system shown in figure 4 was constructed to fit the flow passage boundaries and has 21 streamwise nodal points and 40 radial nodes. In planes of constant azimuth, orthogonal streamlines and velocity potential lines were constructed from a two-dimensional plane incompressible analysis(12). This x-y coordinate system was then rotated about the mixer axis to form the axisymmetric coordinate system. Five reference stations are identified on figure 4 and these correspond to the five experimental survey stations mentioned in the previous section. These are labeled 1, 8, 13, 17, 21 and correspond to the computation nodal point nearest to the probing stations. Station number 1 corresponds to the lobe exit station while station number 21 is the mixer exit station.

Although the mixer geometry is axisymmetric, the flow is three dimensional due to the aximuthal variation of the hot and cold streams. However, due to observed symmetry, only a 1/2 lobed pie-shaped segment of the transverse coordinate surface was considered. The shape of this segment and the extent of typical hot and cold streams at the lobe exit station is shown in figure 5. A comparison between the computational and experimental lobe shape are also shown in figure 5.

B. Flow Angularity Measurements

The three velocity components near the exit plane of the lobes were measured using the flow angularity probes described in the Apparatus section. The flow angularity data were obtained in order to provide information about the mixer inflow conditions. The data were measured in a plane parallel to the exit plane of the lobes (see fig. 2). Data were obtained at six radial locations and four circumferential positions within the measurement domain shown in figure 6. The vectors shown in figure 6 are the resultant of the measured radial and azimuthal velocities in a plane transverse to the mean flow. The data were reflected over another fan-core section assuming symmetry in order to obtain the figure shown. Strong radial flows are evident with outflow in the core and inflow in the fan regions. Data of this type were discussed previously in reference 6 and it was suggested that a vortex-type flow was present at the fan-core interfacial regions. Figure 7 shows the results of data enrichment using a four-point linear interpolation scheme on the flow angularity data. The enrichment was carried out in order to obtain a more complete visual image of the secondary flow structure at the lobe exit plane. It is noted in figure 7 that with data enrichment the vortex structure at the stream interfaces appear very distinctly, and supports the suggestion made in a previous paper(6). This overall secondary flow structure is also consistent with earlier LDV measurements of the three velocity components downstream of the lobe exit plane for a different mixer configuration(7).

C. Representation of the Inlet Flow Field

The secondary flow, i.e., the flow that is generated transverse to the streamwise direction, is highly complex after passing through the curved lobe section. This highly complex nature of the real flow field precludes numerical simulation of both the large scale and small scale structure simply because this information is not available. However, the basic features of the secondary inflow field can be identified experimentally and simulated numerically. This class of secondary inflow representation is labeled generic flow fields, i.e., they attempt to simulate only the large scale secondary flow field structure entering the mixer section by a parametric representation. In contrast to real and generic inflow representation, a third category of inflow conditions labeled ideal are defined. Ideal inflow conditions incorporate no secondary flows entering the mixer passage and are used primarily as baseline conditions. The flow in this case is parallel to the streamwise coordinate of the mesh and was used in the earlier results presented by Povinelli, Anderson and Gerstenmaier.(6)

A generic representation of the large scale flow transverse to the streamwise direction can be conceived as being composed of basically radial outflow in the core passage and radial inflow in fan passage, figure 8. In order to easily describe the secondary velocity vectors in the radial direction a parametric representation was conceived by assuming that the core and fan radial velocities may be represented by the relationship

$$V_{core} = K_c \cdot U_{core}$$

$$V_{fan} = K_f \cdot U_{fan}$$

where K_f and K_c are considered constant over their respective flow fields and U is the streamwise velocity. The experimental data for the mixer nozzle configuration under study suggests that $K_c = 0.25$ and $K_f = -0.20$, i.e., on the average, the radial velocities in the core and fan lobe passages are 25 percent and 20 percent, respectively of the streamwise velocity. The streamwise velocity at each mesh point in the two respective streams was assigned its nondimensional reference value, i.e., $U_{fan}/U_{core} = 0.861$ which was then corrected to account for normal pressure gradients at the initial plane as determined from the axisymmetric potential flow. To account for boundary layers on the lobe, plug and shroud surfaces, the streamwise velocity profiles were further scaled in accordance with an assumed turbulent boundary layer profile and distance from the lobe surface. The temperature field was constructed in the core and fan streams by assuming a total temperature ratio $T_{fan}/T_{core} = 0.74$, which corresponds to the experimental temperature ratio. In addition, an entrance Mach number of 0.45 was assumed.

The initial turbulence quantities were initialized through specification of a length scale and free stream turbulence intensities. These turbulence quantities are assumed to be constant across the shear layer but to vary with distance from the wall. For the calculations presented in this paper, the initial length scale was set at 0.05 of the outer shroud radius and turbulent intensity of both the core and fan streams was set at 5 percent.

Since the radial velocities V_{core} and V_{fan} are scaled with the local streamwise velocity, they decay in the wake of the lobes. Near the plug and shroud walls, however, the radial velocity was modified to decay according to boundary layer theory. This was found to be a very important step since shroud and plug calculations were sensitive to the radial velocity decay near the boundaries. This entire flow field was then "relaxed" or made to satisfy the governing equations according to the procedure described in the Analysis section. It is this relaxed initial flow field that is used as the generic inflow condition in the analysis.

RESULTS

A. Influence of Secondary Flows

The generic inflow velocity vector field constructed according to the procedure described in the previous section is presented in figure 9(a) and exhibits the same secondary flow structure as the numerically enhanced experimental data, figure 7. In the construction of this secondary velocity vector field, the average radial secondary flows were numerically 25 and 20 percent of the streamwise core and fan velocities, respectively. The percentage breakdown establishes the initial magnitude and direction of the secondary flow field, which corresponds to the experimental conditions. Although the computational segment included only one half the lobe segment and one-half the core passage, the computational results presented in figure 9 were reflected to represent two lobe and two fan regions. The secondary velocities presented are normal to the streamwise mesh coordinate. The inflow secondary velocity field shows a very strong vortex pattern aligned with the interface between the fan and core flows similar to the experimentally measured flow field. At station number 8, which is located about half way along the plug, the vortex pattern has condensed into a more circular pattern. This vortex pattern is moving radially outward as can be observed in figures 9(c) through 9(e). At the mixer exit figure 9(e), i.e., station number 21, the vortex is still strong. The radially outward flows near the plug tip, figure 9(c) and 9(d) are associated with reduced flow area between circumferential mesh surfaces as the radius is reduced.

A comparison betwen the measured and computed total temperature signatures at the five measuring stations indicated on figure 4 are presented in figure 10. The development of the horseshoe-shaped total temperature signature identified in reference 6 is clearly evident in figures 10(a) through 10(e). This resulting pattern is caused by the secondary flow field, which sustains itself by the normal static pressure gradients within the mixer nozzle passage. The largest variation between measurement and analysis occurs at station number 8, which is about half-way along the plug surface. The experimental total temperature signature suggests strong cross-flows exsist in the core stream violating the symmetry assumption in the calculational procedure. However, an examination of figure 11, which presents the complete total temperature signature surveyed at station number 8, reveals the adjacent lobe flow did not exhibit this nonsymmetric cross flow characteristic. Thus, substantial lobe-to-lobe variation in the secondary flow patterns were present in this mixer nozzle. Agreement between the total temperature signatures of this second lobe segment and the

analysis is very good. Since this non-symmetric behavior was not simulated in the present calculations, the lobe-to-lobe performance variations could not be evaluated.

A comparison between the measured and computed total temperature distributions at the mixer nozzle exit are presented in figure 12 for six rake positions. The computations were made assuming both the generic inflow conditions (solid line) as well as ideal inflow conditions (dashed line). The calculations for both the generic and ideal inflow conditions used the k-ε turbulence model. The parameter θ is the azimuthal angular position of the survey rake as measured from the fan lobe centerline (0^o) figure 5. A comparison between the calculations using the generic secondary inflow pattern and the measured data show excellent agreement. The very strong influence of the secondary flow structure is seen by comparing the solid with the dashed lines which represent the generic and ideal inflow conditions. A comparison between the ideal and generic total temperature signatures calculated at the nozzle exit station are presented in figure 13. It is apparent from figures 10, 12 and 13 that the characteristic horse-shoe total temperature signature identified in reference 6 resulted from the inflow secondary flow vortex structure established by the initial core and fan streams.

Figure 14 presents a comparison between the measured and computated total pressure distribution at the mixer exit for the same relative rake locations as presented in figure 12. A comparison between the ideal and generic analytical predictions of total pressure did not show the same dramatic differences that were revealed in the total temperature results. In general, agreement between measurement and calculation was reasonably good except near the mixer centerline. The lower experimental total pressure in this region resulted from an initial low pressure region at the bottom of the fan lobe, figure 15, which the generic inflow conditions did not anticipate. It is quite apparent from the total pressure signature presented in figure 15 that the real flow entering the mixer nozzle is highly complex. While including the fan trough total pressure deficit in the generic flow will improve the predictions, the large scale flow structure appears to adequately predict the mixing flow.

B. Influence of Turbulence Models

During the course of this analytical study, it was found that the k-ε turbulence model had a tendency to breakdown resulting in negative dissipation in parts of the flow field. This breakdown in the k-ε turbulence model was associated with the homogenous decay model in the presence of strong convective or secondary flows. In order to study the highly complex pressure driven secondary flows a wake turbulence model was defined (see section on turbulence model).

Presented in figure 16 are the effects of turbulence model assumption on the total temperature distribution at the nozzle exit, station number 21. Shown also on figure 16 are the experimental total temperature data. In general, there were only small differences between the two turbulence model results and those occurred away from the plane of symmetry at azimuthal rake positions of 6.0, 9.0 and 12.0 degrees. The k-ε turbulence model broke down just before the total temperature signature began to wrap-around to form the underside of the horse-shoe pattern, figure 17). The wake turbulence model

had no difficulty in forming this lower loop which was clearly present in the experimental data, figure 10(e).

CONCLUDING REMARKS

A finite difference procedure has been developed to analyze the three dimensional subsonic turbulent flows in turbofan forced mixer nozzles. The method is based on a decomposition of the velocity field into primary and secondary flow components which are determined by solution of the equations governing primary momentum, secondary vorticity, thermal energy and continuity. Experimentally, a strong secondary flow pattern was identified which is associated with the radial inflow and outflow characteristics of the core and fan streams and forms a very strong vortex system aligned with the radial interface between the core and fan regions. A procedure was developed to generate a similar generic secondary flow pattern in terms of two constants representing the average radial outflow or inflow in the core and fan streams as a percentabe of the local streamwise velocity. This description of the initial secondary flow gave excellent agreement with experimental data. By identifying the nature of large scale secondary flow structure and associating it with characteristic mixer nozzle behavior; it is felt that the cause-and-effect relationship between lobe design and nozzle performance can be understood.

The complex secondary flow structure that was found to exist in this forced turbofan mixer nozzle was pressure controlled rather than turbulence controlled and dominated the mixing process. This conclusion is supported by the low sensitivity of both the ideal and generic test cases to the use of either a $k-\varepsilon$ or wake turbulence model.

REFERENCES

1. Kuchar, A.P. and Chamberlin, R., "Scale Model Performance Test Investigation of Exhaust System Mixers for an Energy Efficient Engine (E^3) Propulsion System," AIAA Paper 80-0229, Jan. 1980.

2. Shumpert, P.K., "An Experimental Model Investigation of Turbofan Engine Internal Exhaust Gas Mixer Configurations," AIAA Paper 80-0228, Jan. 1980.

3. Kozlowski, H. and Kraft, J., "Experimental Evaluation of Exhaust Mixers for an Energy Efficient Engine," AIAA Paper 80-1088, June 1980.

4. Birch, S.F., Paynter, G.C., Spalding, D.B., and Tatchell, D.G., "Numerical Modeling of Three-Dimensional Flows in Turbofan Engine Exhaust Nozzles," Journal of Aircraft, Vol. 15, No. 8, Aug. 1978, pp. 489-496.

5. Bowditch, D.N., McNally, W.D., Anderson, B.H., Adamczyk, J.J., and Sockol, P.M., "Computational Fluid Mechanics of Internal Flow," Aeropropulsion 1979, NASA CP-2092, 1979, pp. 187-230.

6. Povinelli, L.A., Anderson, B.H., and Gerstenmaier, W., "Computation of Three-Dimensional Flow in Turbofan Mixers and Comparison with Experimental Data," AIAA Paper 80-0227, Jan. 1980.

7. Patterson, R. and Werle, M.J., "Turbofan Forced Mixer Flow Field," United Technologies Research Center, Monthly Progress Report, UTRC/R79 - 912924-24, July 1979.

8. Briley, W.R. and McDonald, H., "Analysis and Computation of Viscous Subsonic Primary and Secondary Flows," Computational Fluid Dynamics Conference, Williamsburg, Va., July 23-25, 1979, Collection of Technical Papers, AIAA, 1979, pp. 74-88.

9. Kreskovsky, J.P., Briley, W.R., and McDonald, H., "Development of a Method for Computing Three-Dimensional Subsonic Turbulent Flows in Turbofan Lobe Mixers," Scientific Research Associates, Inc., Glastonbury, CT., R79-300006-F, Nov. 1979.

10. Launder, B.E., and Spalding, D.B., "The Numerical Computation of Turbulent Flows," Computer Methods in Applied Mechanics and Engineering, Vol. 3, Mar. 1974, pp. 269-289.

11. Dudzinski, T.J., and Krause, L.N., "Flow-Direction Measurement with Fixed-Position Probes," NASA TM X-1904, 1969.

12. Anderson, O.L., "Finite - Difference Solution for Turbulent Swirling Compressible Flow in Axisymmetric Ducts with Struts," NASA CR-2365, 1974.

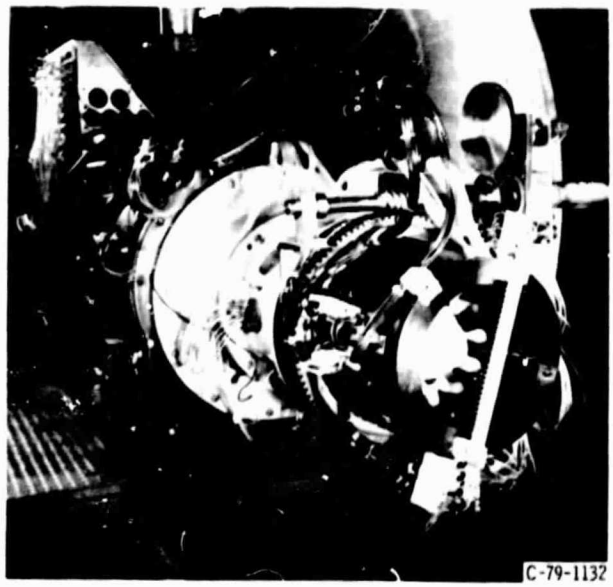

Figure 1. - Experimental mixer nozzle.

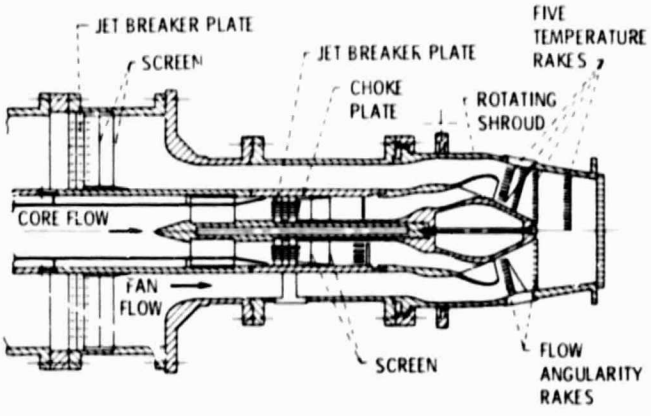

Figure 2. - Mixer nozzle cross-section.

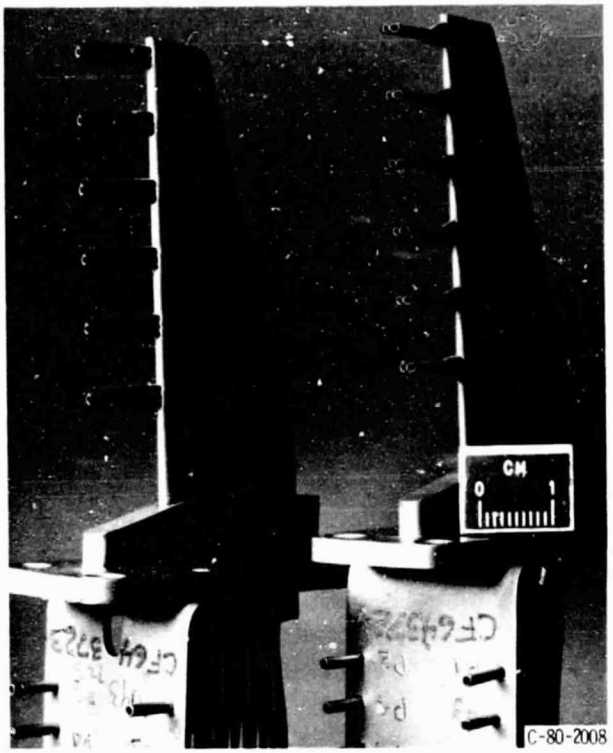

Figure 3. - Flow angularity rates.

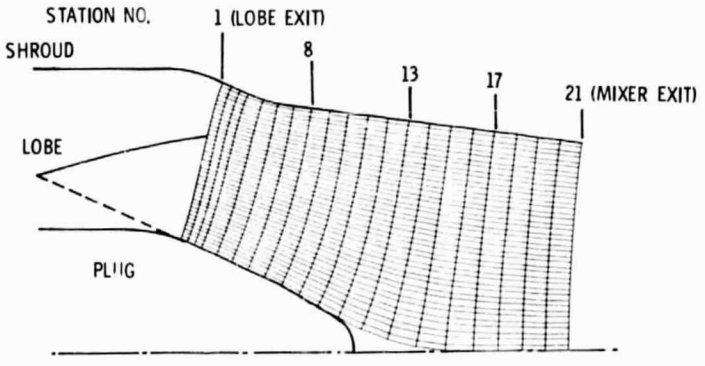

Figure 4. - Mixer nozzle computational mesh.

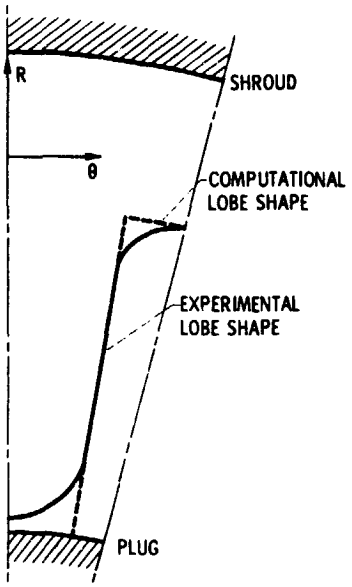

Figure 5. - Transverse computational segment.

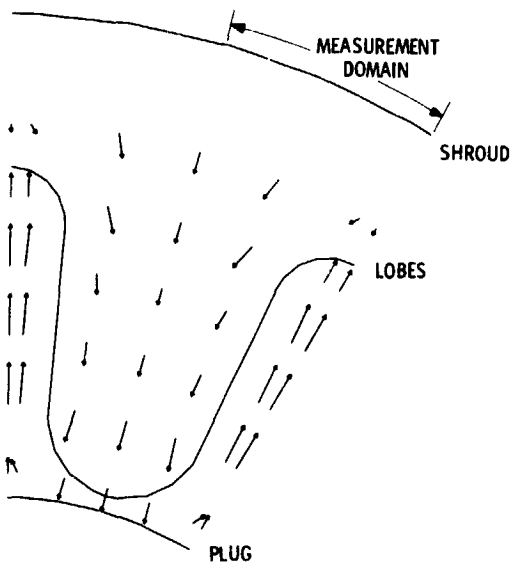

Figure 6. - Measured secondary velocity vectors, lobe exit station.

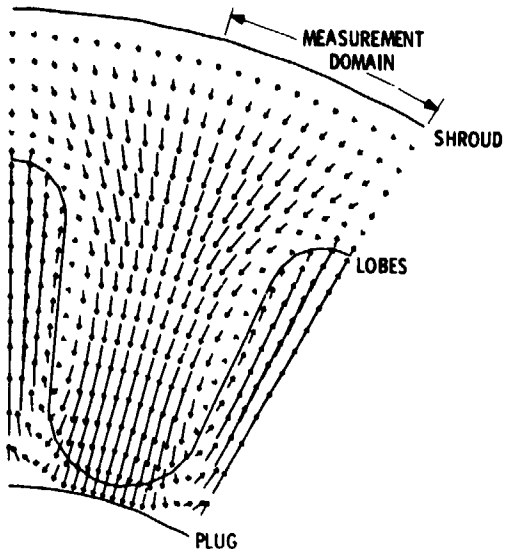

Figure 7. - Enriched measurements of secondary velocity vectors, lobe exit station.

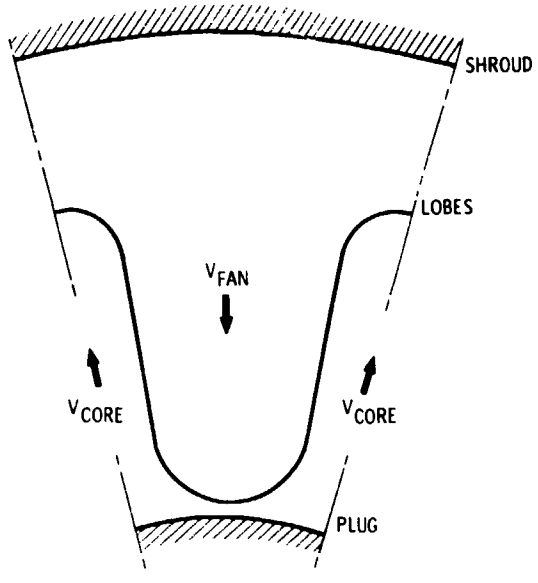

Figure 8. - Large scale basic secondary flow field structure.

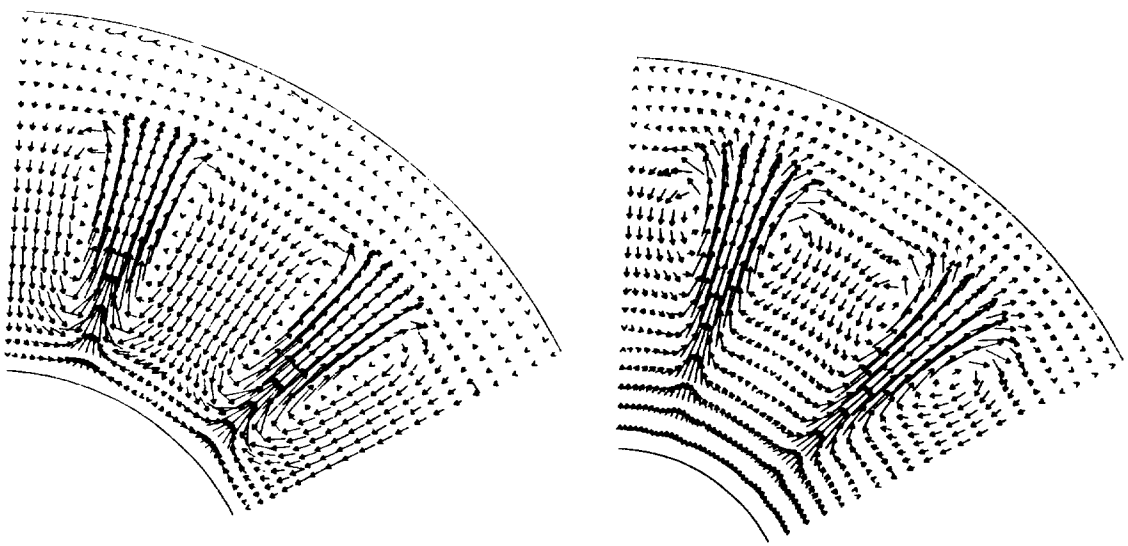

(a) Lobe exit, station no. 1.

(b) Station no. 8.

Figure 9. - Computed secondary velocity vectors.

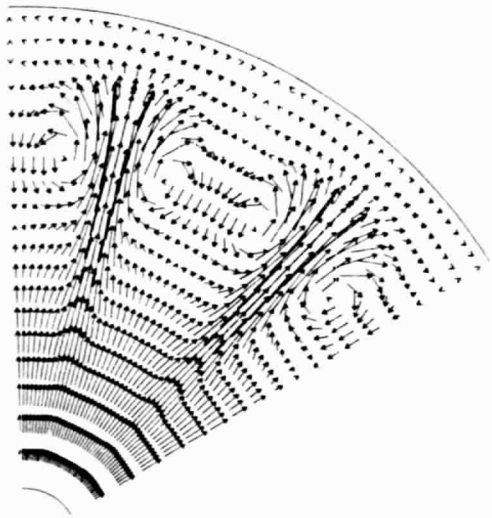

(c) Station no. 13.

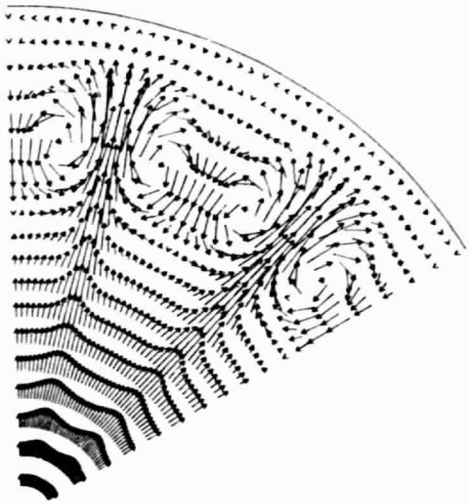

(d) Station no. 17.

Figure 9. - Continued.

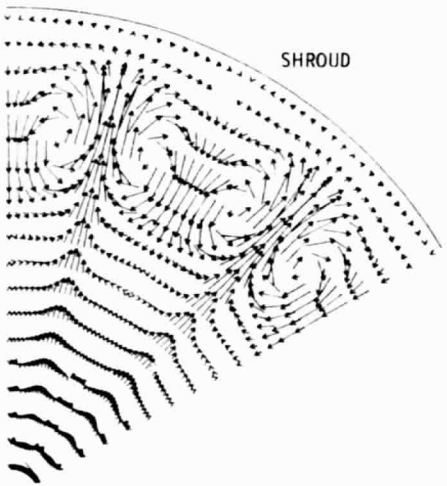

(e) Mixer exit, station no. 21.

Figure 9. - Concluded.

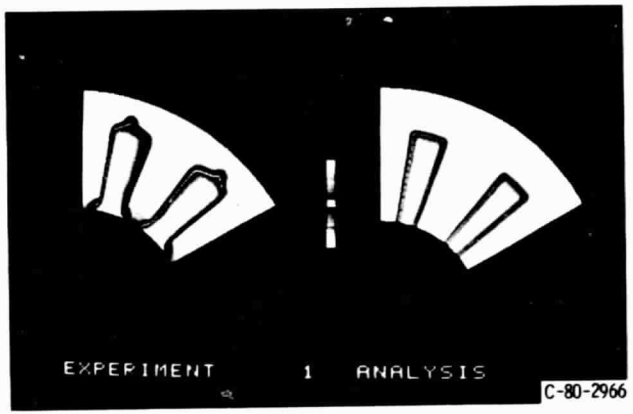

(a) LOBE EXIT, STATION no. 1.

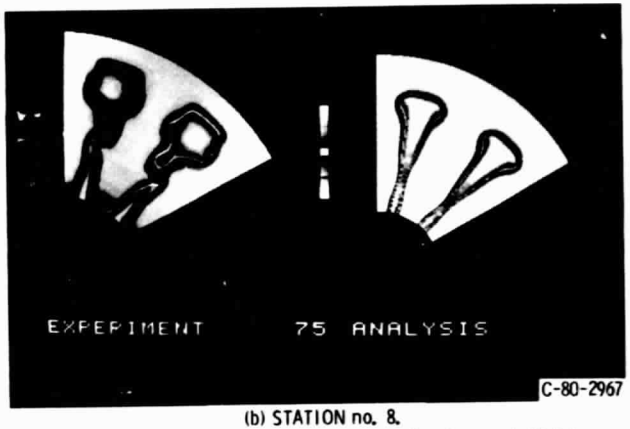

(b) STATION no. 8.

Figure 10. - Comparison between measured and computed total temperature signatures.

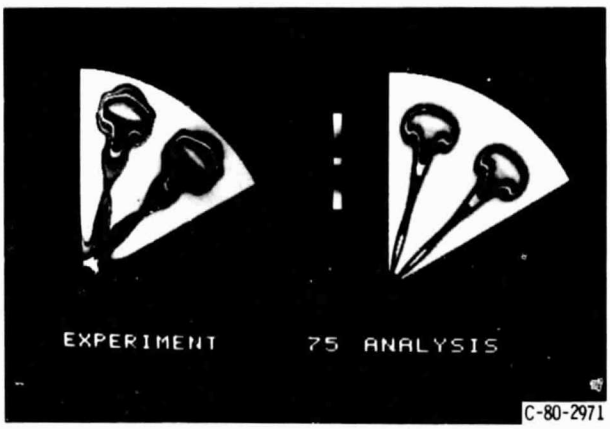

(c) STATION no. 13.

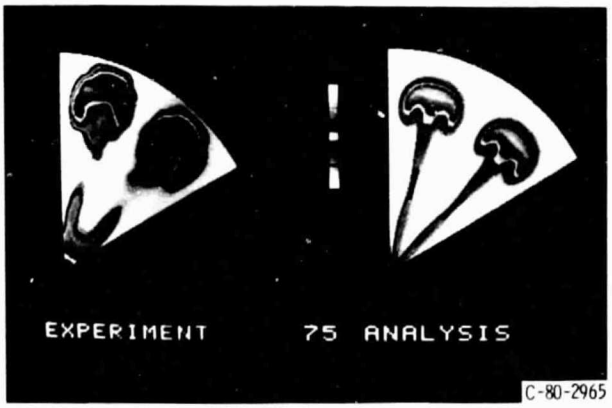

(d) STATION no. 17.

Figure 10. - Continued.

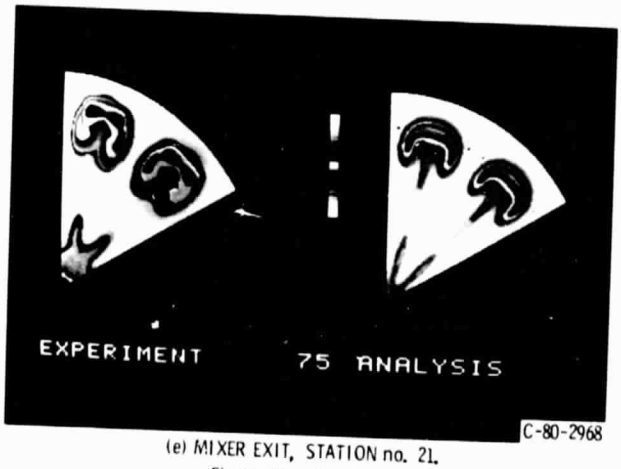

(e) MIXER EXIT, STATION no. 21.

Figure 10. - Concluded.

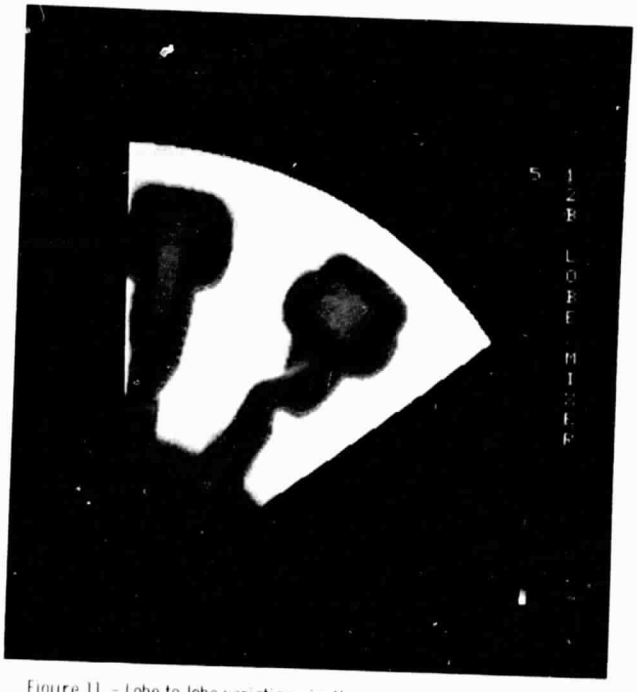

Figure 11. - Lobe to lobe variations in the measured total temperature signature, station no. 8.

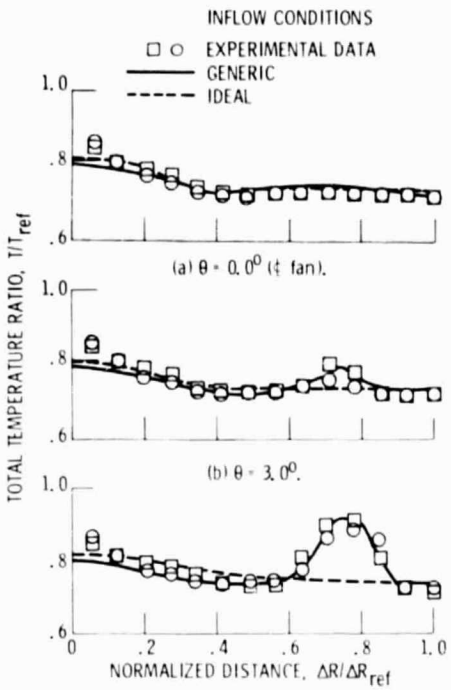

Figure 12. - Effect of inflow conditions on total temperature distribution at the nozzle exit, k-ε turbulence model.

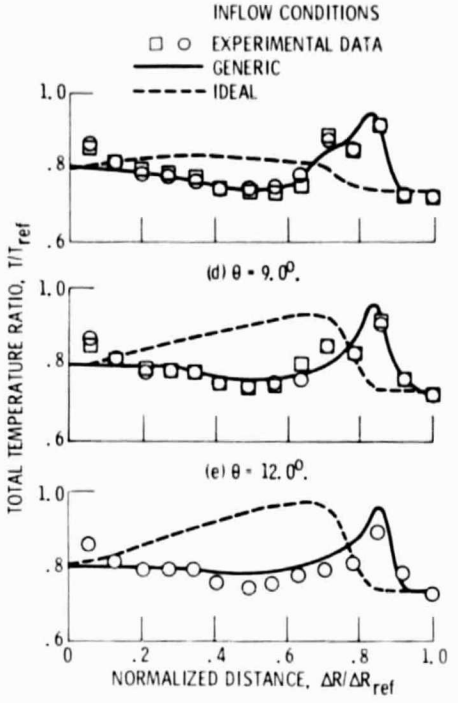

Figure 12. - Concluded.

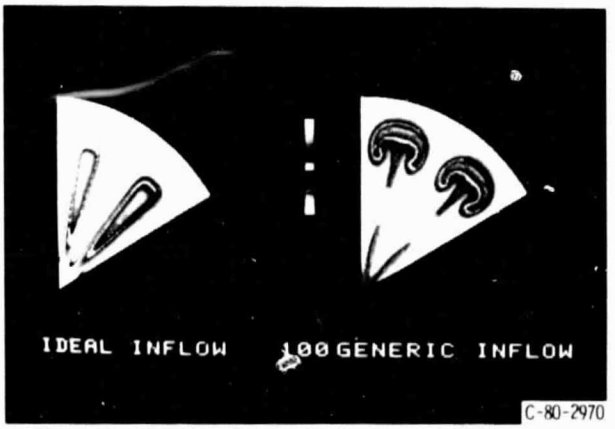

Figure 13. - Comparison between ideal and generic total temperature signatures, mixer exit, station no. 21.

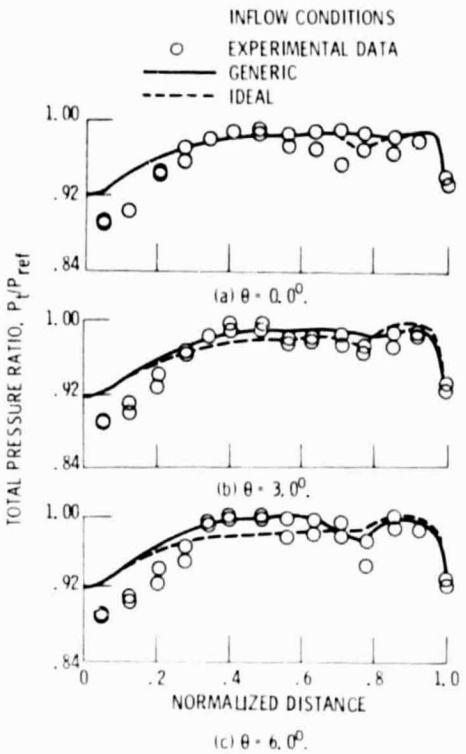

Figure 14. - Effect of inflow conditions on the total pressure distribution at the mixer exit, k-ε turbulence model.

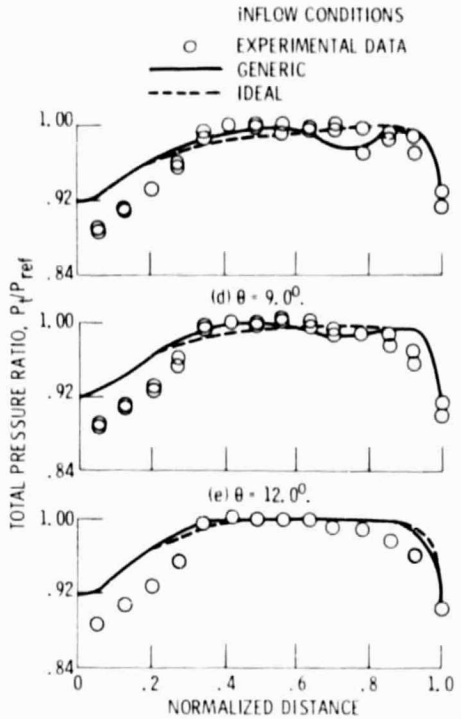

(f) θ = 15.0°.

Figure 14. - Concluded.

Figure 15. - Measure total pressure signature at the lobe exit, station no. 1.

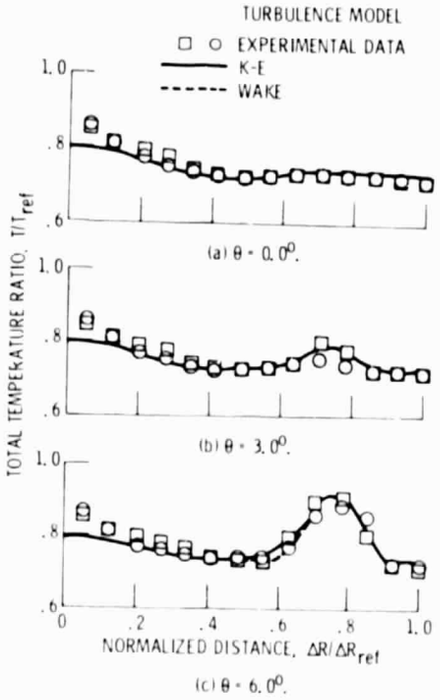

Figure 16. - Effect of turbulence model on total temperature distribution at the nozzle exit, generic inflow conditions.

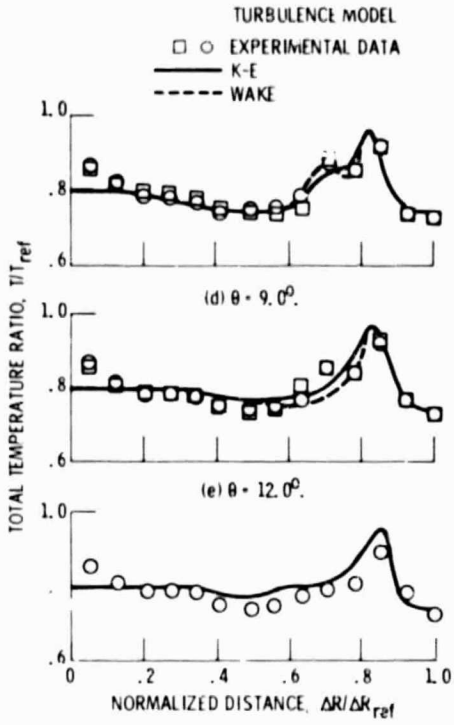

Figure 16. - Concluded.

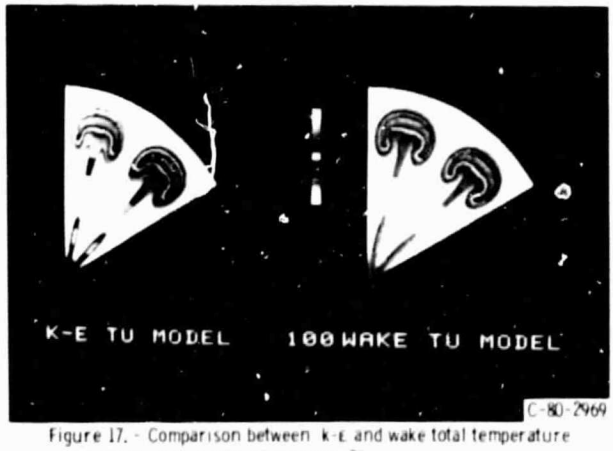

Figure 17. - Comparison between k-ε and wake total temperature signature, mixer exit, station no. 21.